Today's outline - October 16, 2024

Today's outline - October 16, 2024

- Diffuse Scattering

Today's outline - October 16, 2024

- Diffuse Scattering
- Modulated structures

Today's outline - October 16, 2024

- Diffuse Scattering
- Modulated structures
- Lattice vibrations

Today's outline - October 16, 2024

- Diffuse Scattering
- Modulated structures
- Lattice vibrations
- Powder diffraction

Today's outline - October 16, 2024

- Diffuse Scattering
- Modulated structures
- Lattice vibrations
- Powder diffraction
- Pair distribution function

Today's outline - October 16, 2024

- Diffuse Scattering
- Modulated structures
- Lattice vibrations
- Powder diffraction
- Pair distribution function
- Bragg & Laue geometries

Today's outline - October 16, 2024

- Diffuse Scattering
- Modulated structures
- Lattice vibrations
- Powder diffraction
- Pair distribution function
- Bragg & Laue geometries

Reading Assignment: Chapter 6.1-6.2

Today's outline - October 16, 2024

- Diffuse Scattering
- Modulated structures
- Lattice vibrations
- Powder diffraction
- Pair distribution function
- Bragg & Laue geometries

Reading Assignment: Chapter 6.1-6.2

Homework Assignment #04:
Chapter 4: 2,4,6,7,10
due Friday, October 18, 2024

Today's outline - October 16, 2024

- Diffuse Scattering
- Modulated structures
- Lattice vibrations
- Powder diffraction
- Pair distribution function
- Bragg & Laue geometries

Reading Assignment: Chapter 6.1-6.2

Homework Assignment #04:
Chapter 4: 2,4,6,7,10
due Friday, October 18, 2024

Homework Assignment #05:
Chapter 5: 1,3,7,9,10
due Monday, October 28, 2024

Truncation rod review

The CTR profile is sensitive to the termination of the surface. This makes it an ideal probe of electron density of adsorbed species or single atom overlayers.

Truncation rod review

The CTR profile is sensitive to the termination of the surface. This makes it an ideal probe of electron density of adsorbed species or single atom overlayers.

$$F^{total} = F^{CTR} + F^{top\ layer}$$

Truncation rod review

The CTR profile is sensitive to the termination of the surface. This makes it an ideal probe of electron density of adsorbed species or single atom overlayers.

$$F^{total} = F^{CTR} + F^{top\ layer}$$
$$= \frac{A(\vec{Q})}{1 - e^{i2\pi l}}$$

Truncation rod review

The CTR profile is sensitive to the termination of the surface. This makes it an ideal probe of electron density of adsorbed species or single atom overlayers.

$$
\begin{aligned}
F^{total} &= F^{CTR} + F^{top\ layer} \\
&= \frac{A(\vec{Q})}{1 - e^{i2\pi l}} + A(\vec{Q}) e^{-i2\pi(1+z_0)l}
\end{aligned}
$$

Truncation rod review

The CTR profile is sensitive to the termination of the surface. This makes it an ideal probe of electron density of adsorbed species or single atom overlayers.

$$F^{total} = F^{CTR} + F^{top\ layer}$$
$$= \frac{A(\vec{Q})}{1 - e^{i2\pi l}} + A(\vec{Q})e^{-i2\pi(1+z_0)l}$$

where z_0 is the relative displacement of the top layer from the bulk lattice spacing a_3

Truncation rod review

The CTR profile is sensitive to the termination of the surface. This makes it an ideal probe of electron density of adsorbed species or single atom overlayers.

$$F^{total} = F^{CTR} + F^{top\ layer}$$
$$= \frac{A(\vec{Q})}{1 - e^{i2\pi l}} + A(\vec{Q})e^{-i2\pi(1+z_0)l}$$

where z_0 is the relative displacement of the top layer from the bulk lattice spacing a_3

This effect gets larger for larger momentum transfers

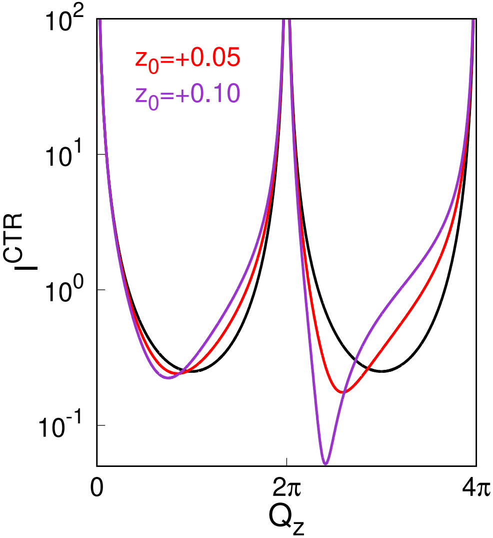

Buried interfaces of Ag films on silicon

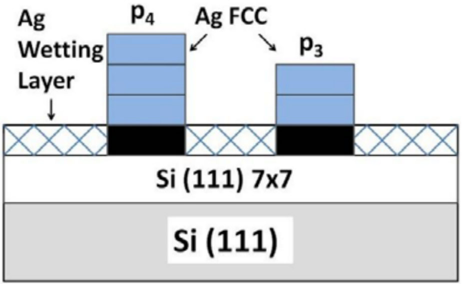

"Critical role of a buried interface in the Stranski-Krastanov growth of metallic nanocrystals: Quantum size effects in Ag/Si(111)-(7×7)," Y. Chen et al. *Phys. Rev. Lett.* **114**, 035501 (2015).

Buried interfaces of Ag films on silicon

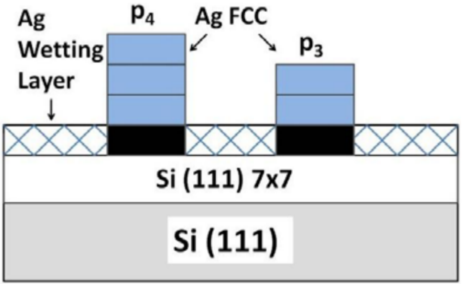

Understanding the process of surface wetting during thin film deposition is crucial to the semiconductor industry

"Critical role of a buried interface in the Stranski-Krastanov growth of metallic nanocrystals: Quantum size effects in Ag/Si(111)-(7×7)," Y. Chen et al. *Phys. Rev. Lett.* **114**, 035501 (2015).

Buried interfaces of Ag films on silicon

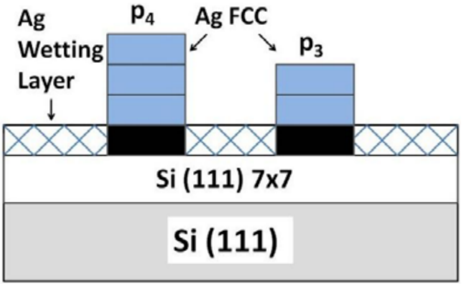

Understanding the process of surface wetting during thin film deposition is crucial to the semiconductor industry

This study uses at *in situ* reflectivity and CTR measurements to study the structural details of Ag film growth on a Si (111) surface

"Critical role of a buried interface in the Stranski-Krastanov growth of metallic nanocrystals: Quantum size effects in Ag/Si(111)-(7×7)," Y. Chen et al. *Phys. Rev. Lett.* **114**, 035501 (2015).

Buried interfaces of Ag films on silicon

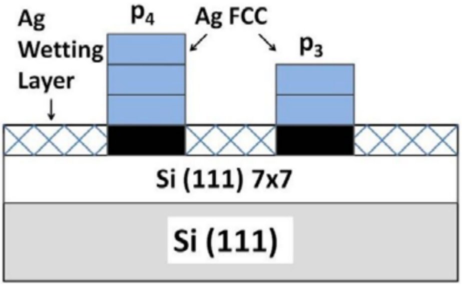

Understanding the process of surface wetting during thin film deposition is crucial to the semiconductor industry

This study uses at *in situ* reflectivity and CTR measurements to study the structural details of Ag film growth on a Si (111) surface

A Si(111) crystal is placed in an ultra-high vacuum chamber and flash-annealed to clean and reconstruct the surface

"Critical role of a buried interface in the Stranski-Krastanov growth of metallic nanocrystals: Quantum size effects in Ag/Si(111)-(7×7)," Y. Chen et al. *Phys. Rev. Lett.* **114**, 035501 (2015).

Buried interfaces of Ag films on silicon

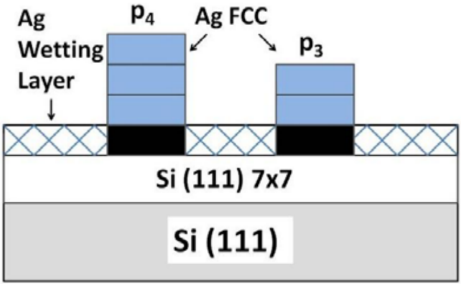

Understanding the process of surface wetting during thin film deposition is crucial to the semiconductor industry

This study uses at *in situ* reflectivity and CTR measurements to study the structural details of Ag film growth on a Si (111) surface

A Si(111) crystal is placed in an ultra-high vacuum chamber and flash-annealed to clean and reconstruct the surface

Ag was thermally evaporated on the surface and both reflectivity measurements of the surface and CTR measurements of the Ag (001) growth layer were performed

"Critical role of a buried interface in the Stranski-Krastanov growth of metallic nanocrystals: Quantum size effects in Ag/Si(111)-(7×7)," Y. Chen et al. *Phys. Rev. Lett.* **114**, 035501 (2015).

Reflectivity & CTR measurements

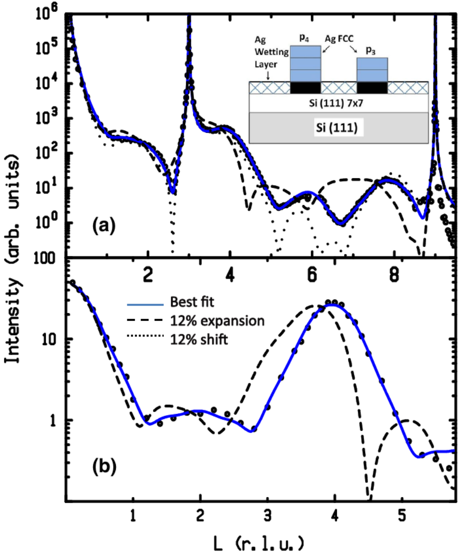

"Critical role of a buried interface in the Stranski-Krastanov growth of metallic nanocrystals: Quantum size effects in Ag/Si(111)-(7×7)," Y. Chen et al. *Phys. Rev. Lett.* **114**, 035501 (2015).

Reflectivity & CTR measurements

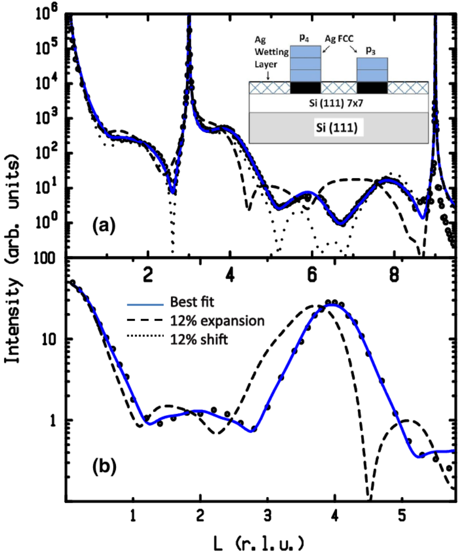

Reflectivity "sees" the entire surface while CTR measures only the incommensurate Ag crystalline layer on the surface

"Critical role of a buried interface in the Stranski-Krastanov growth of metallic nanocrystals: Quantum size effects in Ag/Si(111)-(7×7)," Y. Chen et al. *Phys. Rev. Lett.* **114**, 035501 (2015).

Reflectivity & CTR measurements

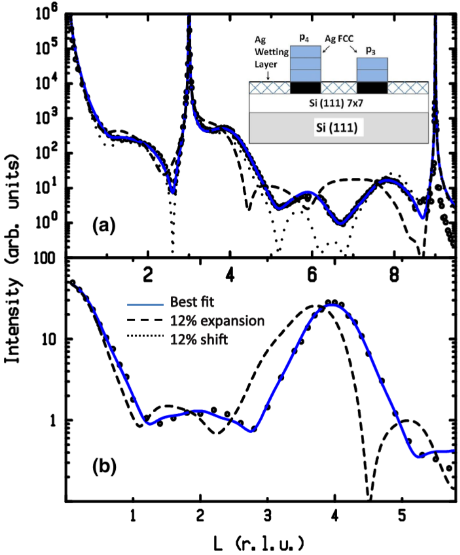

Reflectivity “sees” the entire surface while CTR measures only the incommensurate Ag crystalline layer on the surface

At 0.9 monolayer of Ag the reflectivity shows 3 layers as does the CTR measurement

“Critical role of a buried interface in the Stranski-Krastanov growth of metallic nanocrystals: Quantum size effects in Ag/Si(111)-(7×7),” Y. Chen et al. *Phys. Rev. Lett.* **114**, 035501 (2015).

Reflectivity & CTR measurements

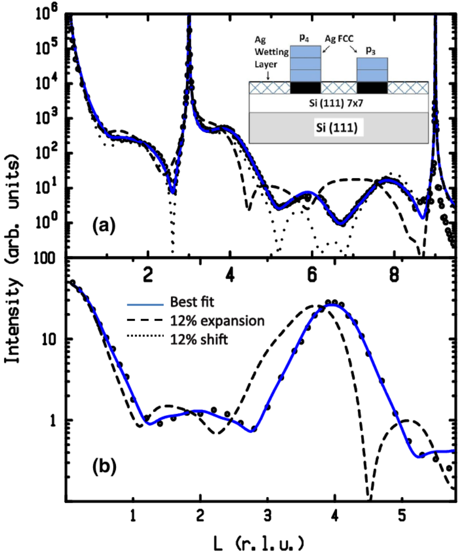

Reflectivity “sees” the entire surface while CTR measures only the incommensurate Ag crystalline layer on the surface

At 0.9 monolayer of Ag the reflectivity shows 3 layers as does the CTR measurement

These results indicate that the islands have an incommensurate Ag fcc structure all the way to the surface while the wetting layer is commensurate with the Si (111)

“Critical role of a buried interface in the Stranski-Krastanov growth of metallic nanocrystals: Quantum size effects in Ag/Si(111)-(7×7),” Y. Chen et al. *Phys. Rev. Lett.* **114**, 035501 (2015).

Reflectivity & CTR measurements

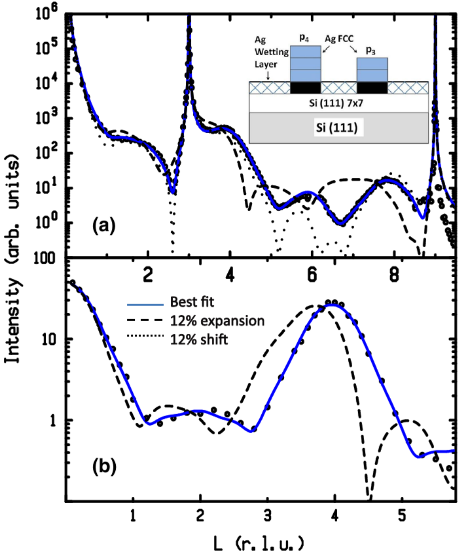

Reflectivity "sees" the entire surface while CTR measures only the incommensurate Ag crystalline layer on the surface

At 0.9 monolayer of Ag the reflectivity shows 3 layers as does the CTR measurement

These results indicate that the islands have an incommensurate Ag fcc structure all the way to the surface while the wetting layer is commensurate with the Si (111)

Modeling shows that the islands are displaced from the surface

"Critical role of a buried interface in the Stranski-Krastanov growth of metallic nanocrystals: Quantum size effects in Ag/Si(111)-(7×7)," Y. Chen et al. *Phys. Rev. Lett.* **114**, 035501 (2015).

Ag island height & quantum confinement

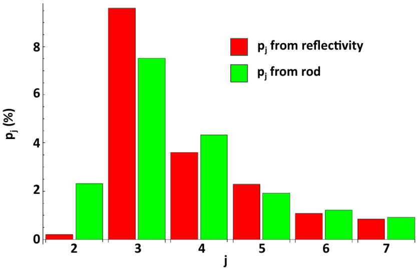

“Critical role of a buried interface in the Stranski-Krastanov growth of metallic nanocrystals: Quantum size effects in Ag/Si(111)-(7×7),” Y. Chen et al. *Phys. Rev. Lett.* **114**, 035501 (2015).

Ag island height & quantum confinement

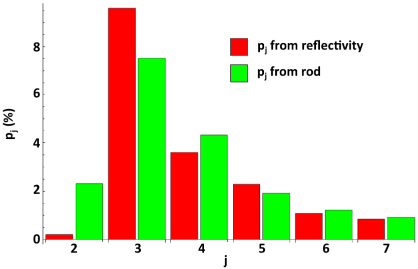

Island layer height distributions from reflectivity and CTR are well correlated and indicate that 3 layers are the minimum for stability

"Critical role of a buried interface in the Stranski-Krastanov growth of metallic nanocrystals: Quantum size effects in Ag/Si(111)-(7×7)," Y. Chen et al. *Phys. Rev. Lett.* **114**, 035501 (2015).

Ag island height & quantum confinement

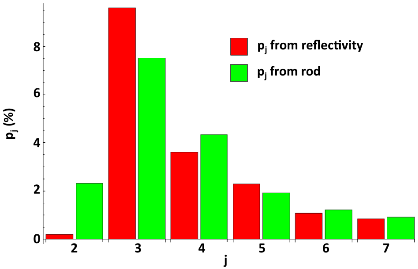

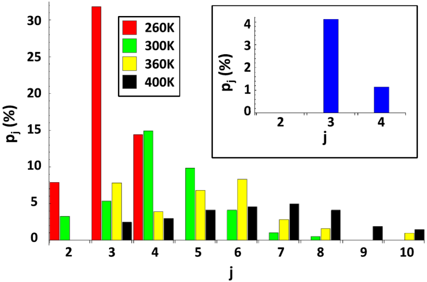

Island layer height distributions from reflectivity and CTR are well correlated and indicate that 3 layers are the minimum for stability

"Critical role of a buried interface in the Stranski-Krastanov growth of metallic nanocrystals: Quantum size effects in Ag/Si(111)-(7×7)," Y. Chen et al. *Phys. Rev. Lett.* **114**, 035501 (2015).

Ag island height & quantum confinement

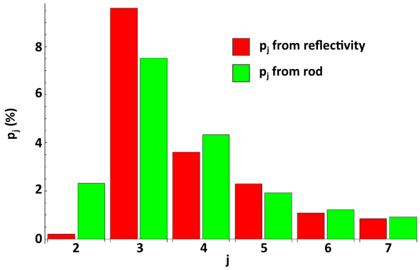

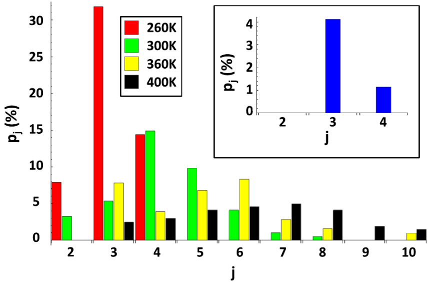

Island layer height distributions from reflectivity and CTR are well correlated and indicate that 3 layers are the minimum for stability

Depositions as a function of temperature show that the island height distribution increases and broadens due to mobility of Ag atoms

"Critical role of a buried interface in the Stranski-Krastanov growth of metallic nanocrystals: Quantum size effects in Ag/Si(111)-(7×7)," Y. Chen et al. *Phys. Rev. Lett.* **114**, 035501 (2015).

Ag island height & quantum confinement

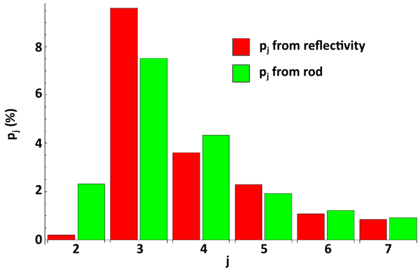

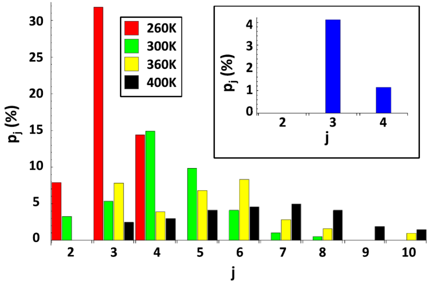

Island layer height distributions from reflectivity and CTR are well correlated and indicate that 3 layers are the minimum for stability

Depositions as a function of temperature show that the island height distribution increases and broadens due to mobility of Ag atoms

The exceptional stability of the three layer islands is consistent with quantum confinement effects that drive the growth process

"Critical role of a buried interface in the Stranski-Krastanov growth of metallic nanocrystals: Quantum size effects in Ag/Si(111)-(7×7)," Y. Chen et al. *Phys. Rev. Lett.* **114**, 035501 (2015).

In plane structure of islands

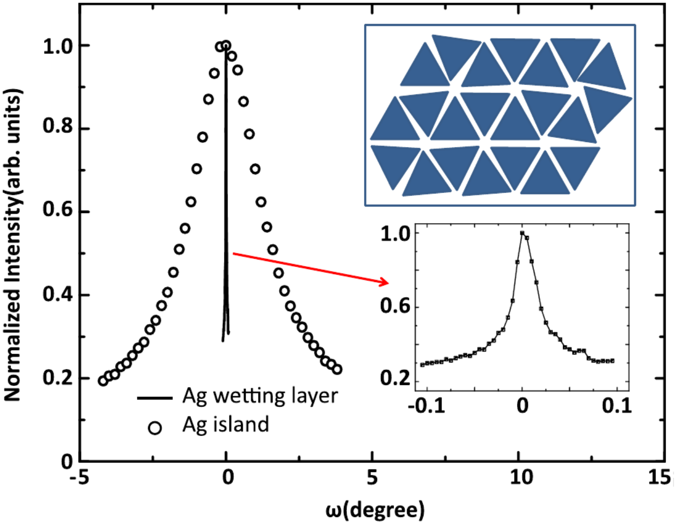

"Critical role of a buried interface in the Stranski-Krastanov growth of metallic nanocrystals: Quantum size effects in Ag/Si(111)-(7×7)," Y. Chen et al. *Phys. Rev. Lett.* **114**, 035501 (2015).

In plane structure of islands

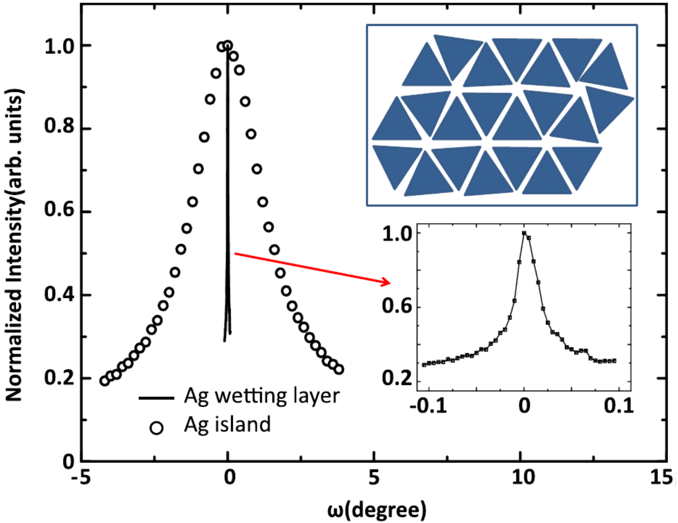

The large in-plane orientational disorder can be seen from the azimuthal scattering profile that is 3 degrees wide

"Critical role of a buried interface in the Stranski-Krastanov growth of metallic nanocrystals: Quantum size effects in Ag/Si(111)-(7×7)," Y. Chen et al. *Phys. Rev. Lett.* **114**, 035501 (2015).

In plane structure of islands

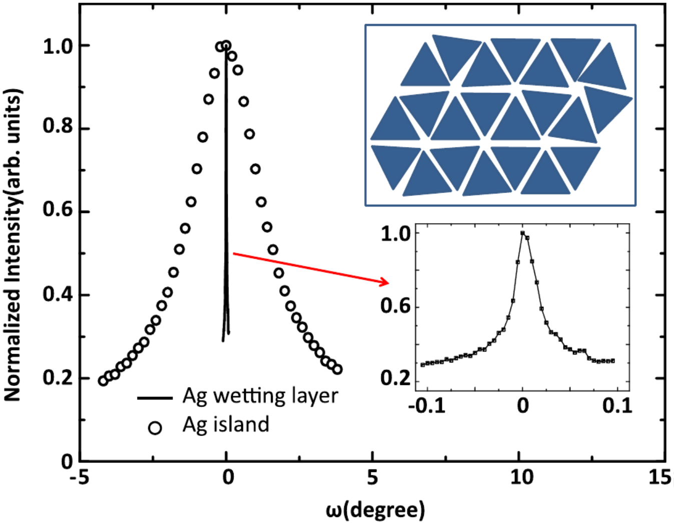

The large in-plane orientational disorder can be seen from the azimuthal scattering profile that is 3 degrees wide The narrow peak is the azimuthal scan of the commensurate wetting layer

"Critical role of a buried interface in the Stranski-Krastanov growth of metallic nanocrystals: Quantum size effects in Ag/Si(111)-(7×7)," Y. Chen et al. *Phys. Rev. Lett.* **114**, 035501 (2015).

In plane structure of islands

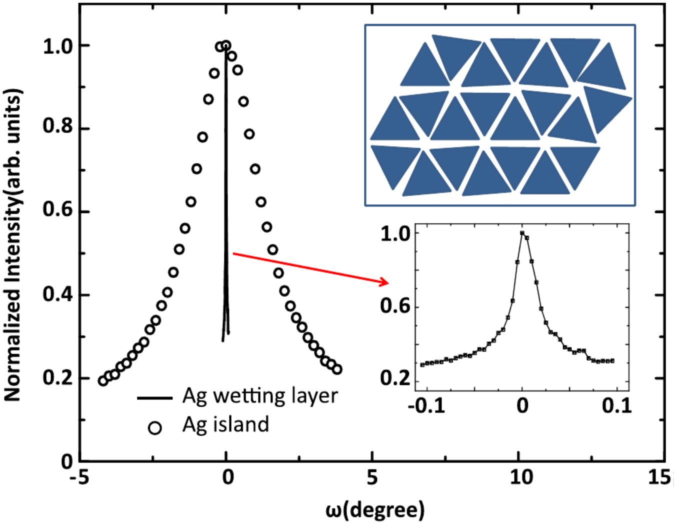

The large in-plane orientational disorder can be seen from the azimuthal scattering profile that is 3 degrees wide The narrow peak is the azimuthal scan of the commensurate wetting layer

The islands thus have a weak interaction with the substrate compared to the wetting layer

"Critical role of a buried interface in the Stranski-Krastanov growth of metallic nanocrystals: Quantum size effects in Ag/Si(111)-(7×7)," Y. Chen et al. *Phys. Rev. Lett.* **114**, 035501 (2015).

Modulated structures

By definition crystals have always been considered to have long range order.

Modulated structures

By definition crystals have always been considered to have long range order.

However, it is common to see structures where the positions of the atoms is modulated (e.g. charge density waves, magnetic lattices, etc.) according to $x_n = an + u\cos(qan)$, where: a is the lattice parameter, u is the amplitude of the displacement, and $q = 2\pi/\lambda_m$ is the wave vector of the modulation.

Modulated structures

By definition crystals have always been considered to have long range order.

However, it is common to see structures where the positions of the atoms is modulated (e.g. charge density waves, magnetic lattices, etc.) according to $x_n = an + u\cos(qan)$, where: a is the lattice parameter, u is the amplitude of the displacement, and $q = 2\pi/\lambda_m$ is the wave vector of the modulation.

If λ_m is a multiple or a rational fraction of a, it is called a commensurate modulation

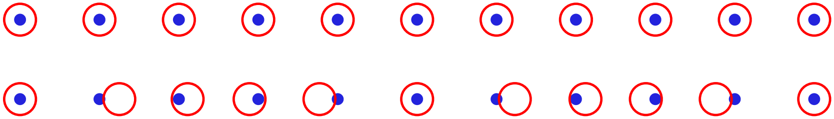

Modulated structures

By definition crystals have always been considered to have long range order.

However, it is common to see structures where the positions of the atoms is modulated (e.g. charge density waves, magnetic lattices, etc.) according to $x_n = an + u\cos(qan)$, where: a is the lattice parameter, u is the amplitude of the displacement, and $q = 2\pi/\lambda_m$ is the wave vector of the modulation.

If λ_m is a multiple or a rational fraction of a, it is called a commensurate modulation but if $\lambda_m = ca$, where c is an irrational number, then it is an incommensurate modulation.

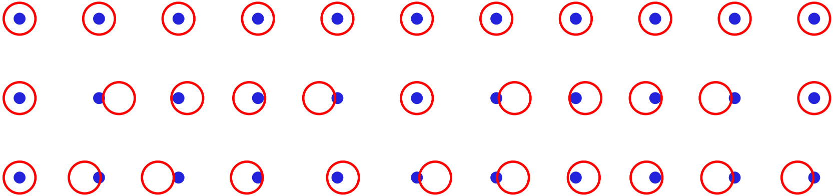

Diffraction from a modulation

For simple a 1D modulated structure, we can compute the scattering

Diffraction from a modulation

For simple a 1D modulated structure, we can compute the scattering

$$A(Q) = \sum_{n=0}^{N-1} e^{iQx_n}$$

Diffraction from a modulation

For simple a 1D modulated structure, we can compute the scattering assuming

$$x_n = an + u\cos(qan)$$

and that the scattering factor for each atom is set to unity

$$A(Q) = \sum_{n=0}^{N-1} e^{iQx_n}$$

Diffraction from a modulation

For simple a 1D modulated structure, we can compute the scattering assuming

$$x_n = an + u\cos(qan)$$

and that the scattering factor for each atom is set to unity

$$A(Q) = \sum_{n=0}^{N-1} e^{iQx_n} = \sum_{n=0}^{N-1} e^{iQ[an+u\cos(qan)]}$$

Diffraction from a modulation

For simple a 1D modulated structure, we can compute the scattering assuming

$$x_n = an + u\cos(qan)$$

and that the scattering factor for each atom is set to unity

$$A(Q) = \sum_{n=0}^{N-1} e^{iQx_n} = \sum_{n=0}^{N-1} e^{iQ[an+u\cos(qan)]}$$
$$= \sum_{n=0}^{N-1} e^{iQan} e^{iQu\cos(qan)}$$

Diffraction from a modulation

For simple a 1D modulated structure, we can compute the scattering assuming

$$x_n = an + u\cos(qan)$$

and that the scattering factor for each atom is set to unity

for the displacement u small, this becomes

$$A(Q) = \sum_{n=0}^{N-1} e^{iQx_n} = \sum_{n=0}^{N-1} e^{iQ[an+u\cos(qan)]}$$

$$= \sum_{n=0}^{N-1} e^{iQan} e^{iQu\cos(qan)}$$

Diffraction from a modulation

For simple a 1D modulated structure, we can compute the scattering assuming

$$x_n = an + u\cos(qan)$$

and that the scattering factor for each atom is set to unity

for the displacement u small, this becomes

$$A(Q) = \sum_{n=0}^{N-1} e^{iQx_n} = \sum_{n=0}^{N-1} e^{iQ[an+u\cos(qan)]}$$

$$= \sum_{n=0}^{N-1} e^{iQan} e^{iQu\cos(qan)}$$

$$A(Q) \approx \sum_{n=0}^{N-1} e^{iQan}\left[1 + iQu\cos(qan) + \cdots\right]$$

Diffraction from a modulation

For simple a 1D modulated structure, we can compute the scattering assuming

$$x_n = an + u\cos(qan)$$

and that the scattering factor for each atom is set to unity

for the displacement u small, this becomes

$$A(Q) = \sum_{n=0}^{N-1} e^{iQx_n} = \sum_{n=0}^{N-1} e^{iQ[an+u\cos(qan)]}$$

$$= \sum_{n=0}^{N-1} e^{iQan} e^{iQu\cos(qan)}$$

$$A(Q) \approx \sum_{n=0}^{N-1} e^{iQan}\left[1 + iQu\cos(qan) + \cdots\right]$$

$$A(Q) \approx \sum_{n=0}^{N-1} e^{iQan} + i\left(\frac{Qu}{2}\right)\left[e^{i(Q+q)an} + e^{-i(Q-q)an}\right]$$

Diffraction from a modulation

For simple a 1D modulated structure, we can compute the scattering assuming

$$x_n = an + u\cos(qan)$$

and that the scattering factor for each atom is set to unity

for the displacement u small, this becomes

$$A(Q) = \sum_{n=0}^{N-1} e^{iQx_n} = \sum_{n=0}^{N-1} e^{iQ[an+u\cos(qan)]}$$

$$= \sum_{n=0}^{N-1} e^{iQan} e^{iQu\cos(qan)}$$

$$A(Q) \approx \sum_{n=0}^{N-1} e^{iQan}\left[1 + iQu\cos(qan) + \cdots\right]$$

$$A(Q) \approx \sum_{n=0}^{N-1} e^{iQan} + i\left(\frac{Qu}{2}\right)\left[e^{i(Q+q)an} + e^{-i(Q-q)an}\right]$$

$$I(Q) = N\left(\frac{2\pi}{a}\right)\sum_h \delta(Q-G_h) + \left(\frac{Qu}{2}\right)^2\left[\delta(Q+q-G_h) + \delta(Q-q-G_h)\right]$$

Diffraction from a modulation

For simple a 1D modulated structure, we can compute the scattering assuming

$$x_n = an + u\cos(qan)$$

and that the scattering factor for each atom is set to unity

for the displacement u small, this becomes

$$A(Q) = \sum_{n=0}^{N-1} e^{iQx_n} = \sum_{n=0}^{N-1} e^{iQ[an+u\cos(qan)]}$$

$$= \sum_{n=0}^{N-1} e^{iQan} e^{iQu\cos(qan)}$$

$$A(Q) \approx \sum_{n=0}^{N-1} e^{iQan}\left[1 + iQu\cos(qan) + \cdots\right]$$

$$A(Q) \approx \sum_{n=0}^{N-1} e^{iQan} + i\left(\frac{Qu}{2}\right)\left[e^{i(Q+q)an} + e^{-i(Q-q)an}\right]$$

$$I(Q) = N\left(\frac{2\pi}{a}\right)\sum_h \delta(Q-G_h) + \left(\frac{Qu}{2}\right)^2\left[\delta(Q+q-G_h) + \delta(Q-q-G_h)\right]$$

the diffraction pattern has main Bragg peaks plus satellite peaks

Quasiperiodic scattering

$$I(Q) = N\left(\frac{2\pi}{a}\right)\sum_h \delta(Q-G_h) + \left(\frac{Qu}{2}\right)^2\left[\delta(Q+q-G_h) + \delta(Q-q-G_h)\right]$$

Quasiperiodic scattering

$$I(Q) = N\left(\frac{2\pi}{a}\right)\sum_h \delta(Q-G_h) + \left(\frac{Qu}{2}\right)^2\left[\delta(Q+q-G_h)+\delta(Q-q-G_h)\right]$$

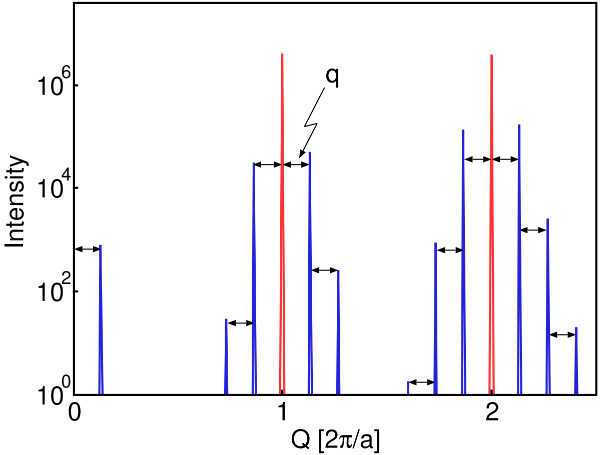

Quasiperiodic scattering

$$I(Q) = N\left(\frac{2\pi}{a}\right)\sum_h \delta(Q-G_h) + \left(\frac{Qu}{2}\right)^2\left[\delta(Q+q-G_h)+\delta(Q-q-G_h)\right]$$

This kind of scattering pattern holds for both commensurate and incommensurate modulations and there are multiple satellites around the $Q=0$ as well as every main peak

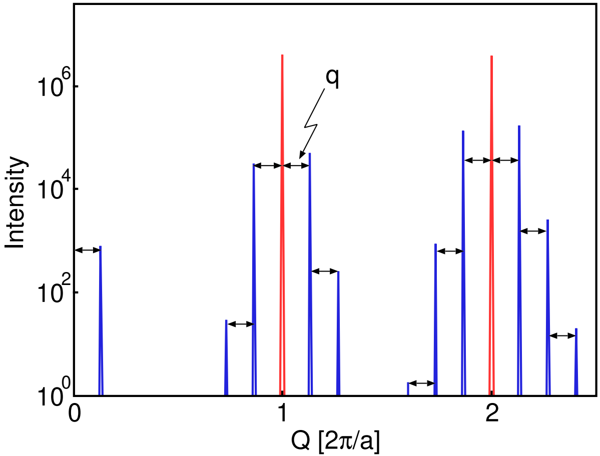

Quasiperiodic scattering

$$I(Q) = N\left(\frac{2\pi}{a}\right)\sum_h \delta(Q-G_h) + \left(\frac{Qu}{2}\right)^2\left[\delta(Q+q-G_h)+\delta(Q-q-G_h)\right]$$

This kind of scattering pattern holds for both commensurate and incommensurate modulations and there are multiple satellites around the $Q = 0$ as well as every main peak

If the modulation of the structure is a multiple of the lattice parameter, the modulation is simply a superlattice and the actual lattice parameter will be changed.

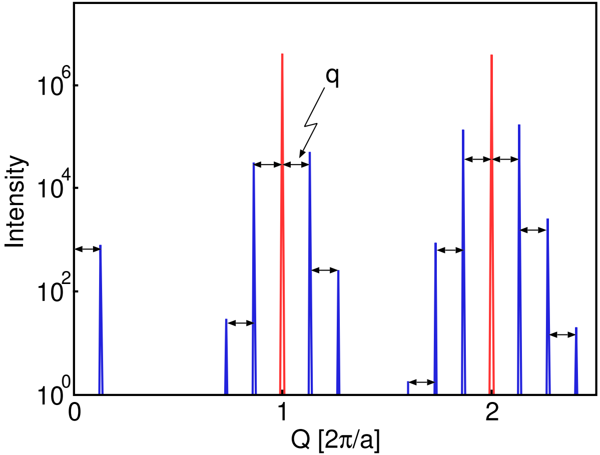

Quasicrystals

The only rotational symmetries which permit a space-filling lattice are 2-, 3-, 4-, and 6-fold.

Quasicrystals

The only rotational symmetries which permit a space-filling lattice are 2-, 3-, 4-, and 6-fold.

In 1984, D. Schechtman and co-workers reported the first observation of a “crystal” with long range order but no translational symmetry in rapidly cooled $Al_{86}Mn_{14}$.

Quasicrystals

The only rotational symmetries which permit a space-filling lattice are 2-, 3-, 4-, and 6-fold.

In 1984, D. Schechtman and co-workers reported the first observation of a “crystal” with long range order but no translational symmetry in rapidly cooled $Al_{86}Mn_{14}$.

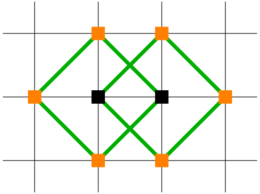

Quasicrystals

The only rotational symmetries which permit a space-filling lattice are 2-, 3-, 4-, and 6-fold.

In 1984, D. Schechtman and co-workers reported the first observation of a “crystal” with long range order but no translational symmetry in rapidly cooled $Al_{86}Mn_{14}$.

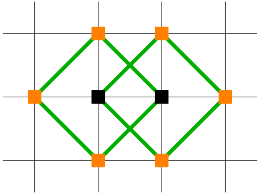

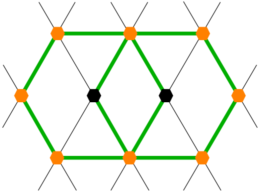

Quasicrystals

The only rotational symmetries which permit a space-filling lattice are 2-, 3-, 4-, and 6-fold.

In 1984, D. Schechtman and co-workers reported the first observation of a "crystal" with long range order but no translational symmetry in rapidly cooled $Al_{86}Mn_{14}$.

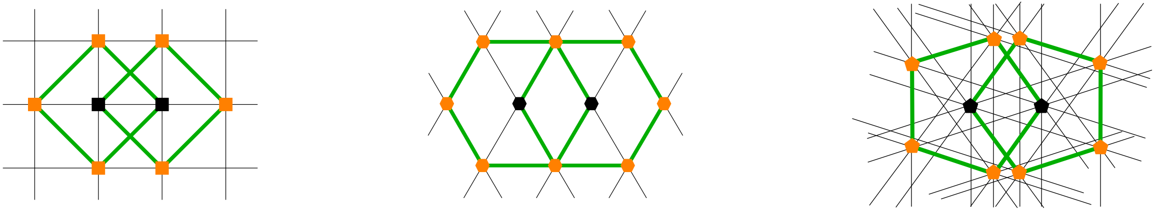

Quasicrystals

The only rotational symmetries which permit a space-filling lattice are 2-, 3-, 4-, and 6-fold.

In 1984, D. Schechtman and co-workers reported the first observation of a "crystal" with long range order but no translational symmetry in rapidly cooled $Al_{86}Mn_{14}$.

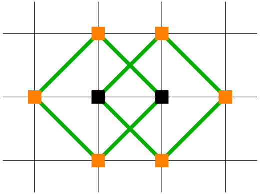

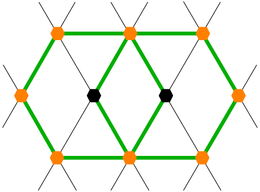

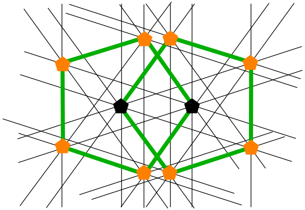

Initially this result was not accepted but as many new materials with the same were discovered it was clear that a new kind of crystal had been discovered.

Quasicrystals

The only rotational symmetries which permit a space-filling lattice are 2-, 3-, 4-, and 6-fold.

In 1984, D. Schechtman and co-workers reported the first observation of a “crystal” with long range order but no translational symmetry in rapidly cooled $Al_{86}Mn_{14}$.

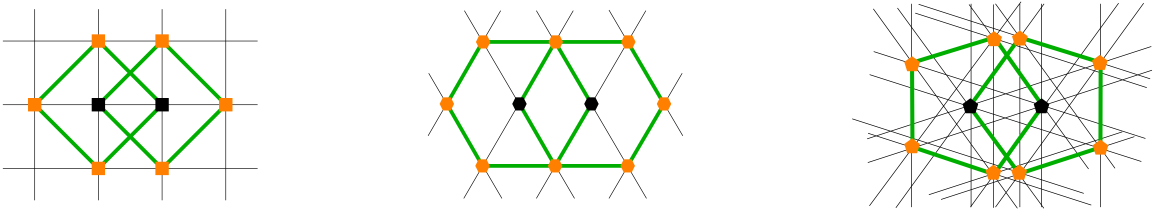

Initially this result was not accepted but as many new materials with the same were discovered it was clear that a new kind of crystal had been discovered.

In 2011 Shechtman was awarded the Nobel Prize in Chemistry

5-fold symmetry

The electron micrographs show that there must be long range order to be able to get such sharp diffraction peaks

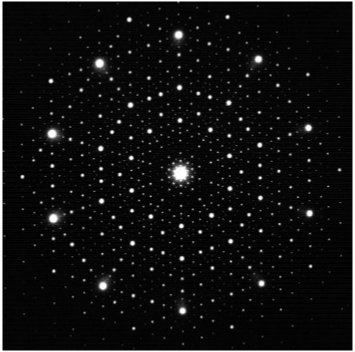

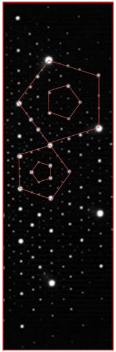

“Metallic phase with long-range orientational order and no translational symmetry,” D. Shechtman, I. Blech, D. Gratias, and J.W. Cahn, *Phys. Rev. Lett.* **53**, 1951-1953 (1984)

5-fold symmetry

The electron micrographs show that there must be long range order to be able to get such sharp diffraction peaks

The 5-fold symmetry is evident in the 10 spots surrounding the center of the left image and the pentagonal arrangements of atoms in the image on the right.

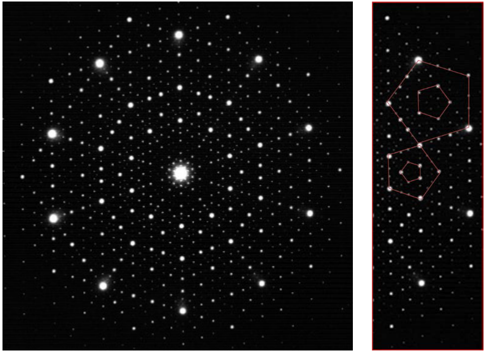

"Metallic phase with long-range orientational order and no translational symmetry," D. Shechtman, I. Blech, D. Gratias, and J.W. Cahn, *Phys. Rev. Lett.* **53**, 1951-1953 (1984)

5-fold symmetry

The electron micrographs show that there must be long range order to be able to get such sharp diffraction peaks

The 5-fold symmetry is evident in the 10 spots surrounding the center of the left image and the pentagonal arrangements of atoms in the image on the right.

This metastable phase was also found with Fe and Cr in the place of Mn.

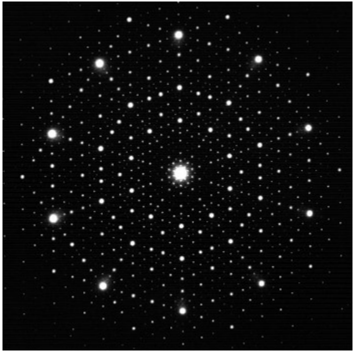

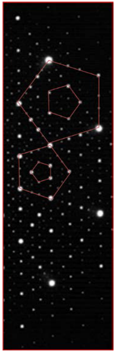

"Metallic phase with long-range orientational order and no translational symmetry," D. Shechtman, I. Blech, D. Gratias, and J.W. Cahn, *Phys. Rev. Lett.* **53**, 1951-1953 (1984)

5-fold symmetry

The electron micrographs show that there must be long range order to be able to get such sharp diffraction peaks

The 5-fold symmetry is evident in the 10 spots surrounding the center of the left image and the pentagonal arrangements of atoms in the image on the right.

This metastable phase was also found with Fe and Cr in the place of Mn.

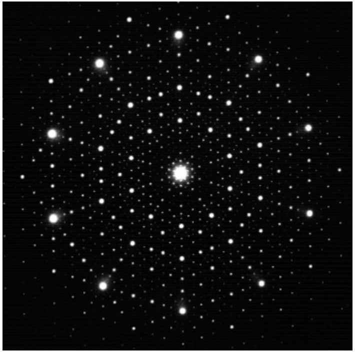

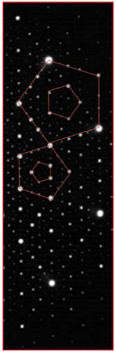

Other groups have discovered stable icosahedral phases with three and two elements.

"Metallic phase with long-range orientational order and no translational symmetry," D. Shechtman, I. Blech, D. Gratias, and J.W. Cahn, *Phys. Rev. Lett.* **53**, 1951-1953 (1984)

Quasicrystal diffraction patterns

The $Al_{65}Cu_{20}Fe_{15}$ system was one of the first stable quasicrystals to be discovered. Later discovery of stable quasicrystals in the Ta-Te, Cd-Ca, and Cd-Yb systems enabled large crystals to be grown.

"A stable quasicrystal in Al-Cu-Fe system," A.-P. Tsai, A. Inoue, and T. Masumoto, *Jap. J. Appl. Phys.* **26**, L1505 (1987)

Quasicrystal diffraction patterns

The $Al_{65}Cu_{20}Fe_{15}$ system was one of the first stable quasicrystals to be discovered. Later discovery of stable quasicrystals in the Ta-Te, Cd-Ca, and Cd-Yb systems enabled large crystals to be grown.

The diffraction pattern and SEM images show the hallmark of an icosahedral crystal

"A stable quasicrystal in Al-Cu-Fe system," A.-P. Tsai, A. Inoue, and T. Masumoto, *Jap. J. Appl. Phys.* **26**, L1505 (1987)

Quasicrystal diffraction patterns

The $Al_{65}Cu_{20}Fe_{15}$ system was one of the first stable quasicrystals to be discovered. Later discovery of stable quasicrystals in the Ta-Te, Cd-Ca, and Cd-Yb systems enabled large crystals to be grown.

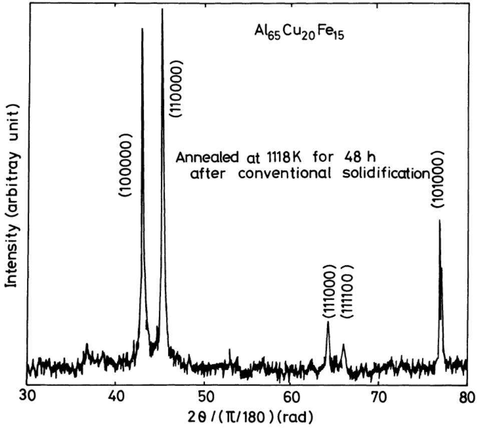

The diffraction pattern and SEM images show the hallmark of an icosahedral crystal

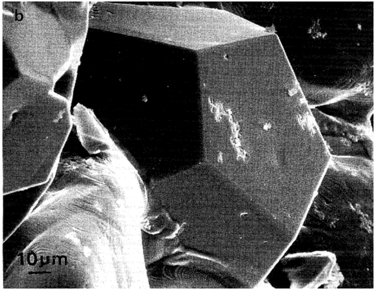

"A stable quasicrystal in Al-Cu-Fe system," A.-P. Tsai, A. Inoue, and T. Masumoto, *Jap. J. Appl. Phys.* **26**, L1505 (1987)

Lattice Vibrations

Atoms on a lattice are not rigid but vibrate. There is zero-point motion as well as thermal motion. These vibrations influence the x-ray scattering.

Lattice Vibrations

Atoms on a lattice are not rigid but vibrate. There is zero-point motion as well as thermal motion. These vibrations influence the x-ray scattering.

For a 1D lattice, we replace the position of the atom with its *instantaneous* position, $\vec{R}_n + \vec{u}_n$ where $\vec{u}_n$ is the displacement from the equilibrium position, $\vec{R}_n$.

Lattice Vibrations

Atoms on a lattice are not rigid but vibrate. There is zero-point motion as well as thermal motion. These vibrations influence the x-ray scattering.

For a 1D lattice, we replace the position of the atom with its *instantaneous* position, $\vec{R}_n + \vec{u}_n$ where $\vec{u}_n$ is the displacement from the equilibrium position, $\vec{R}_n$. Computing the intensity:

Lattice Vibrations

Atoms on a lattice are not rigid but vibrate. There is zero-point motion as well as thermal motion. These vibrations influence the x-ray scattering.

For a 1D lattice, we replace the position of the atom with its *instantaneous* position, $\vec{R}_n + \vec{u}_n$ where $\vec{u}_n$ is the displacement from the equilibrium position, $\vec{R}_n$. Computing the intensity:

$$I = \left\langle \sum_m f(\vec{Q}) e^{i\vec{Q}\cdot(\vec{R}_m+\vec{u}_m)} \sum_n f^*(\vec{Q}) e^{-i\vec{Q}\cdot(\vec{R}_n+\vec{u}_n)} \right\rangle$$

Lattice Vibrations

Atoms on a lattice are not rigid but vibrate. There is zero-point motion as well as thermal motion. These vibrations influence the x-ray scattering.

For a 1D lattice, we replace the position of the atom with its *instantaneous* position, $\vec{R}_n + \vec{u}_n$ where $\vec{u}_n$ is the displacement from the equilibrium position, $\vec{R}_n$. Computing the intensity:

$$I = \left\langle \sum_m f(\vec{Q}) e^{i\vec{Q}\cdot(\vec{R}_m+\vec{u}_m)} \sum_n f^*(\vec{Q}) e^{-i\vec{Q}\cdot(\vec{R}_n+\vec{u}_n)} \right\rangle$$
$$= \sum_m \sum_n f(\vec{Q}) f^*(\vec{Q}) e^{i\vec{Q}\cdot(\vec{R}_m-\vec{R}_n)} \left\langle e^{i\vec{Q}\cdot(\vec{u}_m-\vec{u}_n)} \right\rangle$$

Lattice Vibrations

Atoms on a lattice are not rigid but vibrate. There is zero-point motion as well as thermal motion. These vibrations influence the x-ray scattering.

For a 1D lattice, we replace the position of the atom with its *instantaneous* position, $\vec{R}_n + \vec{u}_n$ where $\vec{u}_n$ is the displacement from the equilibrium position, $\vec{R}_n$. Computing the intensity:

$$\begin{aligned} I &= \left\langle \sum_m f(\vec{Q}) e^{i\vec{Q}\cdot(\vec{R}_m+\vec{u}_m)} \sum_n f^*(\vec{Q}) e^{-i\vec{Q}\cdot(\vec{R}_n+\vec{u}_n)} \right\rangle \\ &= \sum_m \sum_n f(\vec{Q}) f^*(\vec{Q}) e^{i\vec{Q}\cdot(\vec{R}_m-\vec{R}_n)} \left\langle e^{i\vec{Q}\cdot(\vec{u}_m-\vec{u}_n)} \right\rangle \end{aligned}$$

The last term is a time average which can be simplified by first taking the scalar product, $\vec{Q}\cdot\vec{u}_n = u_{Qn}$ to project the displacement along the scattering vector, then applying the Baker-Hausdorff theorem, $\left\langle e^{ix} \right\rangle = e^{-\langle x^2 \rangle/2}$

Lattice Vibrations

Atoms on a lattice are not rigid but vibrate. There is zero-point motion as well as thermal motion. These vibrations influence the x-ray scattering.

For a 1D lattice, we replace the position of the atom with its *instantaneous* position, $\vec{R}_n + \vec{u}_n$ where $\vec{u}_n$ is the displacement from the equilibrium position, $\vec{R}_n$. Computing the intensity:

$$I = \left\langle \sum_m f(\vec{Q}) e^{i\vec{Q}\cdot(\vec{R}_m+\vec{u}_m)} \sum_n f^*(\vec{Q}) e^{-i\vec{Q}\cdot(\vec{R}_n+\vec{u}_n)} \right\rangle$$
$$= \sum_m \sum_n f(\vec{Q}) f^*(\vec{Q}) e^{i\vec{Q}\cdot(\vec{R}_m-\vec{R}_n)} \left\langle e^{i\vec{Q}\cdot(\vec{u}_m-\vec{u}_n)} \right\rangle$$

The last term is a time average which can be simplified by first taking the scalar product, $\vec{Q}\cdot\vec{u}_n = u_{Qn}$ to project the displacement along the scattering vector, then applying the Baker-Hausdorff theorem, $\left\langle e^{ix} \right\rangle = e^{-\langle x^2\rangle/2}$

$$\left\langle e^{i\vec{Q}\cdot(\vec{u}_m-\vec{u}_n)} \right\rangle = \left\langle e^{iQ(u_{Qm}-u_{Qn})} \right\rangle$$

Lattice Vibrations

Atoms on a lattice are not rigid but vibrate. There is zero-point motion as well as thermal motion. These vibrations influence the x-ray scattering.

For a 1D lattice, we replace the position of the atom with its *instantaneous* position, $\vec{R}_n + \vec{u}_n$ where $\vec{u}_n$ is the displacement from the equilibrium position, $\vec{R}_n$. Computing the intensity:

$$I = \left\langle \sum_m f(\vec{Q}) e^{i\vec{Q}\cdot(\vec{R}_m+\vec{u}_m)} \sum_n f^*(\vec{Q}) e^{-i\vec{Q}\cdot(\vec{R}_n+\vec{u}_n)} \right\rangle$$
$$= \sum_m \sum_n f(\vec{Q}) f^*(\vec{Q}) e^{i\vec{Q}\cdot(\vec{R}_m-\vec{R}_n)} \left\langle e^{i\vec{Q}\cdot(\vec{u}_m-\vec{u}_n)} \right\rangle$$

The last term is a time average which can be simplified by first taking the scalar product, $\vec{Q}\cdot\vec{u}_n = u_{Qn}$ to project the displacement along the scattering vector, then applying the Baker-Hausdorff theorem, $\left\langle e^{ix} \right\rangle = e^{-\langle x^2 \rangle/2}$

$$\left\langle e^{i\vec{Q}\cdot(\vec{u}_m-\vec{u}_n)} \right\rangle = \left\langle e^{iQ(u_{Qm}-u_{Qn})} \right\rangle = e^{-\langle Q^2(u_{Qm}-u_{Qn})^2 \rangle/2}$$

Lattice Vibrations

$$\left\langle e^{iQ(u_{Qm}-u_{Qn})}\right\rangle = e^{-Q^2\langle u_{Qm}^2\rangle/2}e^{-Q^2\langle u_{Qn}^2\rangle/2}e^{Q^2\langle u_{Qm}u_{Qn}\rangle}$$

Lattice Vibrations

$$\left\langle e^{iQ(u_{Qm}-u_{Qn})}\right\rangle = e^{-Q^2\langle u_{Qm}^2\rangle/2} e^{-Q^2\langle u_{Qn}^2\rangle/2} e^{Q^2\langle u_{Qm}u_{Qn}\rangle}$$

$$= e^{-Q^2\langle u_Q^2\rangle} e^{Q^2\langle u_{Qm}u_{Qn}\rangle}$$

Lattice Vibrations

$$
\begin{aligned}
\left\langle e^{iQ(u_{Qm}-u_{Qn})}\right\rangle &= e^{-Q^2\langle u_{Qm}^2\rangle/2} e^{-Q^2\langle u_{Qn}^2\rangle/2} e^{Q^2\langle u_{Qm}u_{Qn}\rangle} \\
&= e^{-Q^2\langle u_Q^2\rangle} e^{Q^2\langle u_{Qm}u_{Qn}\rangle} = e^{-2M} e^{Q^2\langle u_{Qm}u_{Qn}\rangle}
\end{aligned}
$$

Lattice Vibrations

$$\left\langle e^{iQ(u_{Qm}-u_{Qn})} \right\rangle = e^{-Q^2\langle u_{Qm}^2\rangle/2} e^{-Q^2\langle u_{Qn}^2\rangle/2} e^{Q^2\langle u_{Qm}u_{Qn}\rangle}$$
$$= e^{-Q^2\langle u_Q^2\rangle} e^{Q^2\langle u_{Qm}u_{Qn}\rangle} = e^{-2M} e^{Q^2\langle u_{Qm}u_{Qn}\rangle} = e^{-2M}\left[1 + e^{Q^2\langle u_{Qm}u_{Qn}\rangle} - 1\right]$$

Lattice Vibrations

$$\left\langle e^{iQ(u_{Qm}-u_{Qn})}\right\rangle = e^{-Q^2\langle u_{Qm}^2\rangle/2}e^{-Q^2\langle u_{Qn}^2\rangle/2}e^{Q^2\langle u_{Qm}u_{Qn}\rangle}$$
$$= e^{-Q^2\langle u_Q^2\rangle}e^{Q^2\langle u_{Qm}u_{Qn}\rangle} = e^{-2M}e^{Q^2\langle u_{Qm}u_{Qn}\rangle} = e^{-2M}\left[1 + e^{Q^2\langle u_{Qm}u_{Qn}\rangle} - 1\right]$$

Substituting into the expression for intensity

Lattice Vibrations

$$\left\langle e^{iQ(u_{Qm}-u_{Qn})}\right\rangle = e^{-Q^2\langle u_{Qm}^2\rangle/2} e^{-Q^2\langle u_{Qn}^2\rangle/2} e^{Q^2\langle u_{Qm}u_{Qn}\rangle}$$

$$= e^{-Q^2\langle u_Q^2\rangle} e^{Q^2\langle u_{Qm}u_{Qn}\rangle} = e^{-2M} e^{Q^2\langle u_{Qm}u_{Qn}\rangle} = e^{-2M}\left[1 + e^{Q^2\langle u_{Qm}u_{Qn}\rangle} - 1\right]$$

Substituting into the expression for intensity

$$I = \sum_m \sum_n f(\vec{Q}) e^{-M} e^{i\vec{Q}\cdot\vec{R}_m} f^*(\vec{Q}) e^{-M} e^{-i\vec{Q}\cdot\vec{R}_n}$$

$$+ \sum_m \sum_n f(\vec{Q}) e^{-M} e^{i\vec{Q}\cdot\vec{R}_m} f^*(\vec{Q}) e^{-M} e^{-i\vec{Q}\cdot\vec{R}_n} \left[e^{Q^2\langle u_{Qm}u_{Qn}\rangle} - 1\right]$$

Lattice Vibrations

$$\left\langle e^{iQ(u_{Qm}-u_{Qn})}\right\rangle = e^{-Q^2\langle u_{Qm}^2\rangle/2} e^{-Q^2\langle u_{Qn}^2\rangle/2} e^{Q^2\langle u_{Qm}u_{Qn}\rangle}$$

$$= e^{-Q^2\langle u_Q^2\rangle} e^{Q^2\langle u_{Qm}u_{Qn}\rangle} = e^{-2M} e^{Q^2\langle u_{Qm}u_{Qn}\rangle} = e^{-2M}\left[1 + e^{Q^2\langle u_{Qm}u_{Qn}\rangle} - 1\right]$$

Substituting into the expression for intensity

$$I = \sum_m \sum_n f(\vec{Q})e^{-M} e^{i\vec{Q}\cdot\vec{R}_m} f^*(\vec{Q})e^{-M} e^{-i\vec{Q}\cdot\vec{R}_n}$$
$$+ \sum_m \sum_n f(\vec{Q})e^{-M} e^{i\vec{Q}\cdot\vec{R}_m} f^*(\vec{Q})e^{-M} e^{-i\vec{Q}\cdot\vec{R}_n}\left[e^{Q^2\langle u_{Qm}u_{Qn}\rangle} - 1\right]$$

The first term is just the elastic scattering from the lattice with the addition of the term $e^{-M} = e^{-Q^2\langle u_Q^2\rangle/2}$, called the Debye-Waller factor.

Lattice Vibrations

$$\left\langle e^{iQ(u_{Qm}-u_{Qn})} \right\rangle = e^{-Q^2\langle u_{Qm}^2\rangle/2} e^{-Q^2\langle u_{Qn}^2\rangle/2} e^{Q^2\langle u_{Qm}u_{Qn}\rangle}$$
$$= e^{-Q^2\langle u_Q^2\rangle} e^{Q^2\langle u_{Qm}u_{Qn}\rangle} = e^{-2M} e^{Q^2\langle u_{Qm}u_{Qn}\rangle} = e^{-2M}\left[1 + e^{Q^2\langle u_{Qm}u_{Qn}\rangle} - 1\right]$$

Substituting into the expression for intensity

$$I = \sum_m \sum_n f(\vec{Q}) e^{-M} e^{i\vec{Q}\cdot\vec{R}_m} f^*(\vec{Q}) e^{-M} e^{-i\vec{Q}\cdot\vec{R}_n}$$
$$+ \sum_m \sum_n f(\vec{Q}) e^{-M} e^{i\vec{Q}\cdot\vec{R}_m} f^*(\vec{Q}) e^{-M} e^{-i\vec{Q}\cdot\vec{R}_n} \left[e^{Q^2\langle u_{Qm}u_{Qn}\rangle} - 1\right]$$

The first term is just the elastic scattering from the lattice with the addition of the term $e^{-M} = e^{-Q^2\langle u_Q^2\rangle/2}$, called the Debye-Waller factor.

The second term is the Thermal Diffuse Scattering and actually increases with mean squared displacement.

Thermal Diffuse Scattering

$$I^{TDS} = \sum_m \sum_n f(\vec{Q})e^{-M}e^{i\vec{Q}\cdot\vec{R}_m} f^*(\vec{Q})e^{-M}e^{-i\vec{Q}\cdot\vec{R}_n}\left[e^{Q^2\langle u_{Qm}u_{Qn}\rangle} - 1\right]$$

Thermal Diffuse Scattering

$$I^{TDS} = \sum_m \sum_n f(\vec{Q}) e^{-M} e^{i\vec{Q}\cdot\vec{R}_m} f^*(\vec{Q}) e^{-M} e^{-i\vec{Q}\cdot\vec{R}_n} \left[e^{Q^2 \langle u_{Qm} u_{Qn} \rangle} - 1 \right]$$

The TDS has a width determined by the correlated displacement of atoms which is much broader than a Bragg peak.

Thermal Diffuse Scattering

$$I^{TDS} = \sum_m \sum_n f(\vec{Q}) e^{-M} e^{i\vec{Q}\cdot\vec{R}_m} f^*(\vec{Q}) e^{-M} e^{-i\vec{Q}\cdot\vec{R}_n} \left[e^{Q^2 \langle u_{Qm} u_{Qn} \rangle} - 1 \right]$$

The TDS has a width determined by the correlated displacement of atoms which is much broader than a Bragg peak.

These correlated motions are just phonons.

Thermal Diffuse Scattering

$$I^{TDS} = \sum_m \sum_n f(\vec{Q}) e^{-M} e^{i\vec{Q}\cdot\vec{R}_m} f^*(\vec{Q}) e^{-M} e^{-i\vec{Q}\cdot\vec{R}_n} \left[e^{Q^2 \langle u_{Qm} u_{Qn} \rangle} - 1 \right]$$

The TDS has a width determined by the correlated displacement of atoms which is much broader than a Bragg peak.

These correlated motions are just phonons.

A 0.5mm Si wafer illuminated by 28keV x-rays from an APS undulator were used to measure the phonon dispersion curves of silicon

Thermal Diffuse Scattering

$$I^{TDS} = \sum_m \sum_n f(\vec{Q}) e^{-M} e^{i\vec{Q}\cdot\vec{R}_m} f^*(\vec{Q}) e^{-M} e^{-i\vec{Q}\cdot\vec{R}_n} \left[e^{Q^2 \langle u_{Qm} u_{Qn} \rangle} - 1 \right]$$

The TDS has a width determined by the correlated displacement of atoms which is much broader than a Bragg peak.

These correlated motions are just phonons.

A 0.5mm Si wafer illuminated by 28keV x-rays from an APS undulator were used to measure the phonon dispersion curves of silicon

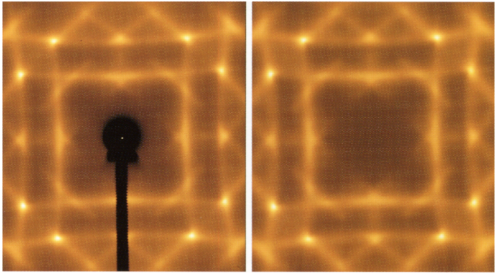

incident beam along (100)

"Determination of phonon dispersions from x-ray transmission scattering: The example of silicon," M. Holt, et al. *Phys. Rev. Lett.* **83**, 3317 (1999).

Thermal Diffuse Scattering

$$I^{TDS} = \sum_m \sum_n f(\vec{Q})e^{-M}e^{i\vec{Q}\cdot\vec{R}_m} f^*(\vec{Q})e^{-M}e^{-i\vec{Q}\cdot\vec{R}_n}\left[e^{Q^2\langle u_{Qm}u_{Qn}\rangle} - 1\right]$$

The TDS has a width determined by the correlated displacement of atoms which is much broader than a Bragg peak.

These correlated motions are just phonons.

A 0.5mm Si wafer illuminated by 28keV x-rays from an APS undulator were used to measure the phonon dispersion curves of silicon

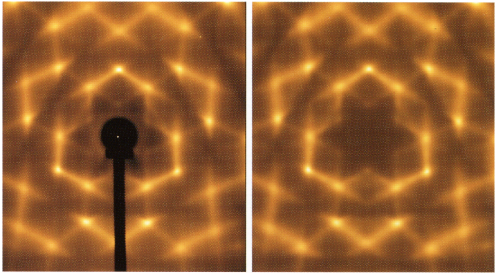

incident beam along (111)

"Determination of phonon dispersions from x-ray transmission scattering: The example of silicon," M. Holt, et al. *Phys. Rev. Lett.* **83**, 3317 (1999).

Thermal Diffuse Scattering

$$I^{TDS} = \sum_m \sum_n f(\vec{Q}) e^{-M} e^{i\vec{Q}\cdot\vec{R}_m} f^*(\vec{Q}) e^{-M} e^{-i\vec{Q}\cdot\vec{R}_n} \left[e^{Q^2\langle u_{Qm} u_{Qn}\rangle} - 1 \right]$$

The TDS has a width determined by the correlated displacement of atoms which is much broader than a Bragg peak.

These correlated motions are just phonons.

A 0.5mm Si wafer illuminated by 28keV x-rays from an APS undulator were used to measure the phonon dispersion curves of silicon

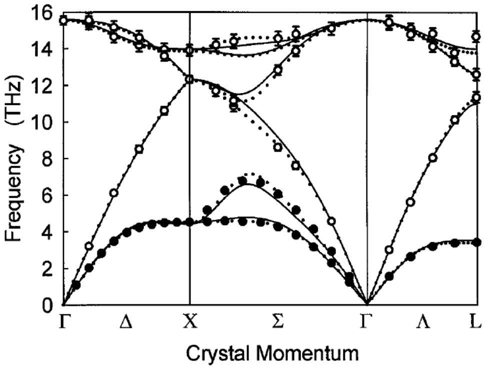

dotted line from this measurement

"Determination of phonon dispersions from x-ray transmission scattering: The example of silicon," M. Holt, et al. *Phys. Rev. Lett.* **83**, 3317 (1999).

Properties of the Debye-Waller Factor

For crystals with several different types of atoms, we generalize the unit cell scattering factor.

Properties of the Debye-Waller Factor

For crystals with several different types of atoms, we generalize the unit cell scattering factor.

$$F^{u.c.} = \sum_j f_j(\vec{Q}) e^{-M_j} e^{i\vec{Q}\cdot\vec{r}_j}$$

Properties of the Debye-Waller Factor

For crystals with several different types of atoms, we generalize the unit cell scattering factor.

$$F^{u.c.} = \sum_j f_j(\vec{Q}) e^{-M_j} e^{i\vec{Q}\cdot\vec{r}_j}$$

$$M_j = \frac{1}{2} Q^2 \langle u_{Qj}^2 \rangle$$

Properties of the Debye-Waller Factor

For crystals with several different types of atoms, we generalize the unit cell scattering factor.

$$F^{u.c.} = \sum_j f_j(\vec{Q}) e^{-M_j} e^{i\vec{Q}\cdot\vec{r}_j}$$

$$M_j = \frac{1}{2} Q^2 \langle u_{Qj}^2 \rangle = \frac{1}{2} \left(\frac{4\pi}{\lambda} \right)^2 \sin^2\theta \langle u_{Qj}^2 \rangle$$

Properties of the Debye-Waller Factor

For crystals with several different types of atoms, we generalize the unit cell scattering factor.

$$B_T^j = 8\pi^2 \langle u_{Qj}^2 \rangle$$

$$F^{u.c.} = \sum_j f_j(\vec{Q}) e^{-M_j} e^{i\vec{Q}\cdot\vec{r}_j}$$

$$M_j = \frac{1}{2} Q^2 \langle u_{Qj}^2 \rangle = \frac{1}{2} \left(\frac{4\pi}{\lambda} \right)^2 \sin^2\theta \langle u_{Qj}^2 \rangle$$

$$M_j = B_T^j \left(\frac{\sin\theta}{\lambda} \right)^2$$

Properties of the Debye-Waller Factor

For crystals with several different types of atoms, we generalize the unit cell scattering factor.

$$B_T^j = 8\pi^2 \langle u_{Qj}^2 \rangle$$

for isotropic atomic vibrations

$$\langle u^2 \rangle = \langle u_x^2 + u_y^2 + u_z^2 \rangle$$
$$= 3\langle u_x^2 \rangle = 3\langle u_Q^2 \rangle$$

$$F^{u.c.} = \sum_j f_j(\vec{Q}) e^{-M_j} e^{i\vec{Q}\cdot\vec{r}_j}$$

$$M_j = \frac{1}{2} Q^2 \langle u_{Qj}^2 \rangle = \frac{1}{2} \left(\frac{4\pi}{\lambda} \right)^2 \sin^2\theta \langle u_{Qj}^2 \rangle$$

$$M_j = B_T^j \left(\frac{\sin\theta}{\lambda} \right)^2$$

Properties of the Debye-Waller Factor

For crystals with several different types of atoms, we generalize the unit cell scattering factor.

$$B_T^j = 8\pi^2 \langle u_{Qj}^2 \rangle$$

for isotropic atomic vibrations

$$\langle u^2 \rangle = \langle u_x^2 + u_y^2 + u_z^2 \rangle$$
$$= 3\langle u_x^2 \rangle = 3\langle u_Q^2 \rangle$$

$$F^{u.c.} = \sum_j f_j(\vec{Q}) e^{-M_j} e^{i\vec{Q}\cdot\vec{r}_j}$$

$$M_j = \frac{1}{2} Q^2 \langle u_{Qj}^2 \rangle = \frac{1}{2} \left(\frac{4\pi}{\lambda} \right)^2 \sin^2\theta \langle u_{Qj}^2 \rangle$$

$$M_j = B_T^j \left(\frac{\sin\theta}{\lambda} \right)^2$$

$$B_T^{iso} = \frac{8\pi^2}{3} \langle u^2 \rangle$$

Properties of the Debye-Waller Factor

For crystals with several different types of atoms, we generalize the unit cell scattering factor.

$$B_T^j = 8\pi^2 \langle u_{Qj}^2 \rangle$$

for isotropic atomic vibrations

$$\begin{aligned} \langle u^2 \rangle &= \langle u_x^2 + u_y^2 + u_z^2 \rangle \\ &= 3\langle u_x^2 \rangle = 3\langle u_Q^2 \rangle \end{aligned}$$

$$F^{u.c.} = \sum_j f_j(\vec{Q}) e^{-M_j} e^{i\vec{Q}\cdot\vec{r}_j}$$

$$M_j = \frac{1}{2} Q^2 \langle u_{Qj}^2 \rangle = \frac{1}{2} \left(\frac{4\pi}{\lambda} \right)^2 \sin^2\theta \langle u_{Qj}^2 \rangle$$

$$M_j = B_T^j \left(\frac{\sin\theta}{\lambda} \right)^2$$

$$B_T^{iso} = \frac{8\pi^2}{3} \langle u^2 \rangle$$

In general, Debye-Waller factors can be anisotropic

The Debye Model

The Debye model can be used to compute B_T by integrating a linear phonon dispersion relation up to a cutoff frequency, ω_D, called the Debye frequency.

The Debye Model

The Debye model can be used to compute B_T by integrating a linear phonon dispersion relation up to a cutoff frequency, ω_D, called the Debye frequency.

B_T is given as a function of the Debye temperature Θ.

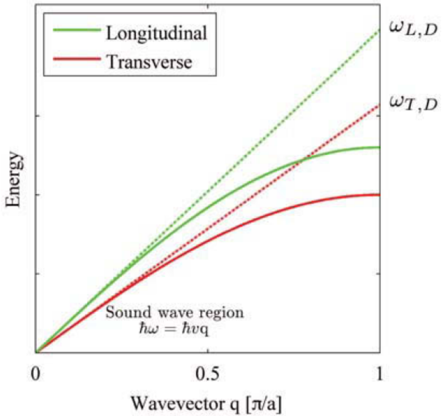

The Debye Model

The Debye model can be used to compute B_T by integrating a linear phonon dispersion relation up to a cutoff frequency, ω_D, called the Debye frequency.

B_T is given as a function of the Debye temperature Θ.

$$B_T = \frac{6h^2}{m_A k_B \Theta}\left[\frac{\phi(\Theta/T)}{\Theta/T} + \frac{1}{4}\right]$$

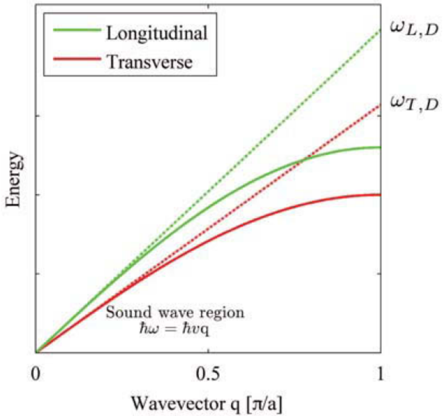

The Debye Model

The Debye model can be used to compute B_T by integrating a linear phonon dispersion relation up to a cutoff frequency, ω_D, called the Debye frequency.

B_T is given as a function of the Debye temperature Θ.

$$B_T = \frac{6h^2}{m_A k_B \Theta}\left[\frac{\phi(\Theta/T)}{\Theta/T} + \frac{1}{4}\right]$$

$$\phi(x) = \frac{1}{x}\int_0^{\Theta/T} \frac{\xi}{e^{\xi}-1}d\xi$$

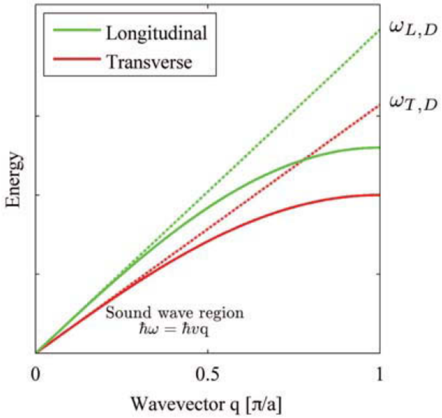

The Debye Model

The Debye model can be used to compute B_T by integrating a linear phonon dispersion relation up to a cutoff frequency, ω_D, called the Debye frequency.

B_T is given as a function of the Debye temperature Θ.

$$B_T = \frac{6h^2}{m_A k_B \Theta}\left[\frac{\phi(\Theta/T)}{\Theta/T} + \frac{1}{4}\right]$$

$$\phi(x) = \frac{1}{x}\int_0^{\Theta/T} \frac{\xi}{e^{\xi}-1}d\xi$$

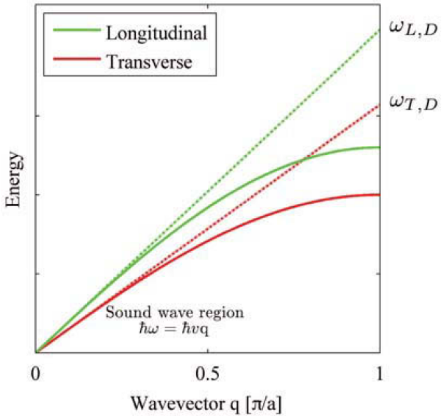

$$B_T[\text{Å}^2] = \frac{11492\text{T[K]}}{\text{A}\Theta^2[\text{K}^2]}\phi(\Theta/\text{T}) + \frac{2873}{\text{A}\Theta[\text{K}]}$$

Debye Temperatures

	A	Θ (K)	$B_{4.2}$	B_{77} (Å^2)	B_{293}
C*	12	2230	0.11	0.11	0.12
Al	27	428	0.25	0.30	0.72
Cu	63.5	343	0.13	0.17	0.47

*diamond

$$B_T = \frac{11492\,T}{A\Theta^2}\phi(\Theta/T) + \frac{2873}{A\Theta}$$

Debye Temperatures

	A	Θ (K)	$B_{4.2}$	B_{77} ($Å^2$)	B_{293}
C*	12	2230	0.11	0.11	0.12
Al	27	428	0.25	0.30	0.72
Cu	63.5	343	0.13	0.17	0.47

*diamond

$$B_T = \frac{11492\,T}{A\Theta^2}\phi(\Theta/T) + \frac{2873}{A\Theta}$$

diamond is very stiff and B_T does not vary much with temperature

Debye Temperatures

	A	Θ (K)	$B_{4.2}$	B_{77} (Å^2)	B_{293}
C*	12	2230	0.11	0.11	0.12
Al	27	428	0.25	0.30	0.72
Cu	63.5	343	0.13	0.17	0.47

*diamond

$$B_T = \frac{11492\,T}{A\Theta^2}\phi(\Theta/T) + \frac{2873}{A\Theta}$$

diamond is very stiff and B_T does not vary much with temperature

copper has a much lower Debye temperature and a wider variation of thermal factor with temperature

Debye Temperatures

	A	Θ (K)	$B_{4.2}$	B_{77} (Å^2)	B_{293}
C*	12	2230	0.11	0.11	0.12
Al	27	428	0.25	0.30	0.72
Cu	63.5	343	0.13	0.17	0.47

*diamond

diamond is very stiff and B_T does not vary much with temperature

copper has a much lower Debye temperature and a wider variation of thermal factor with temperature

$$B_T = \frac{11492\,T}{A\Theta^2}\phi(\Theta/T) + \frac{2873}{A\Theta}$$

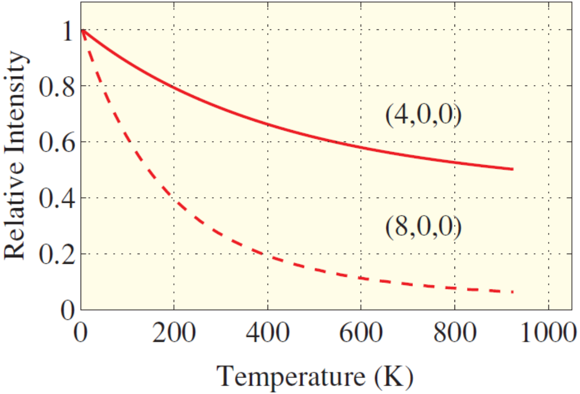

Beamline 11BM at the APS

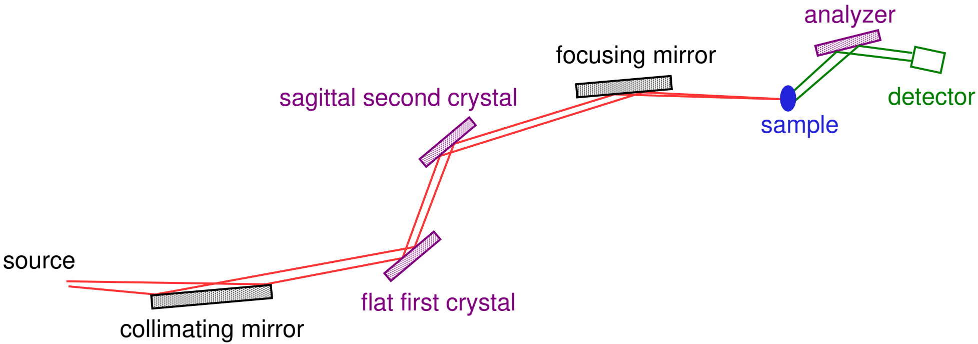

"A dedicated powder diffraction beamline at the Advanced Photon Source: Commissioning and early operational results," J. Wang et al. *Rev. Sci. Instrum.* **79**, 085105 (2008).

Beamline 11BM at the APS

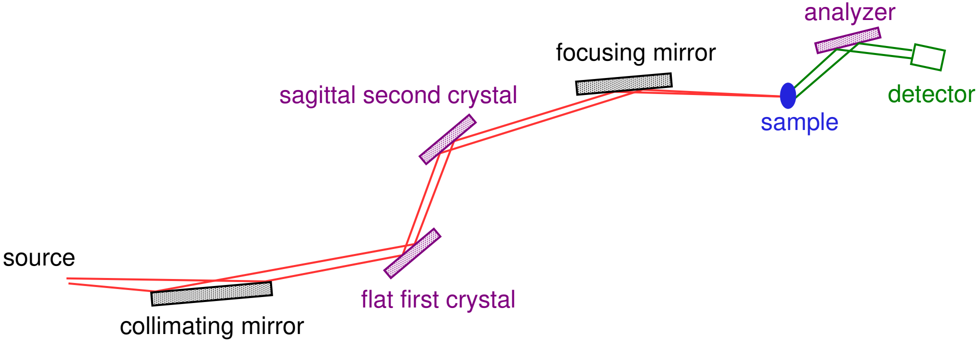

2D detectors have limited angular resolution, for high resolution routine powder diffraction, beamlines such as 11BM are ideal

"A dedicated powder diffraction beamline at the Advanced Photon Source: Commissioning and early operational results," J. Wang et al. *Rev. Sci. Instrum.* **79**, 085105 (2008).

Beamline 11BM at the APS

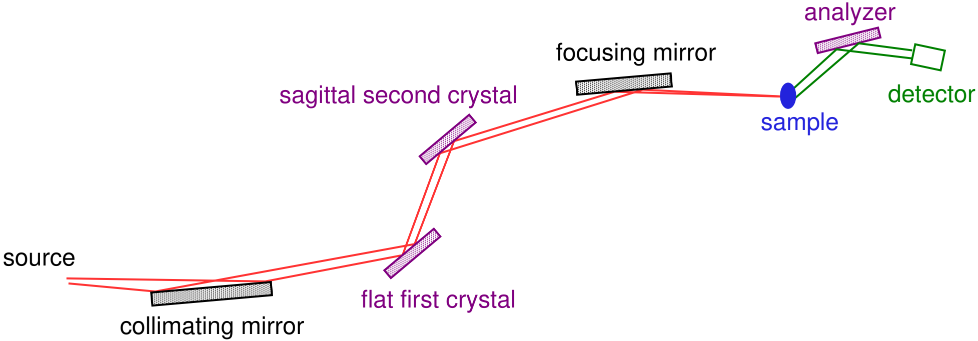

2D detectors have limited angular resolution, for high resolution routine powder diffraction, beamlines such as 11BM are ideal

The initial collimating mirror makes the beam more parallel and then it is focused horizontally and vertically to the sample

"A dedicated powder diffraction beamline at the Advanced Photon Source: Commissioning and early operational results," J. Wang et al. *Rev. Sci. Instrum.* **79**, 085105 (2008).

The high resolution analyzer

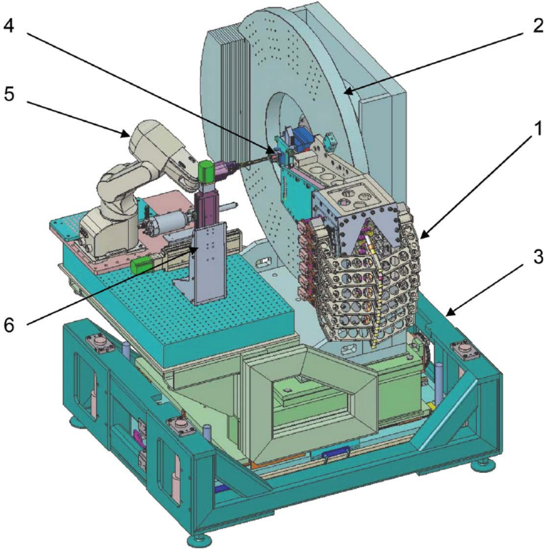

"A twelve-analyzer detector system for high resolution powder diffraction," P.L. Lee et al. *J. Synch. Rad.* **15**, 427-432

The high resolution analyzer

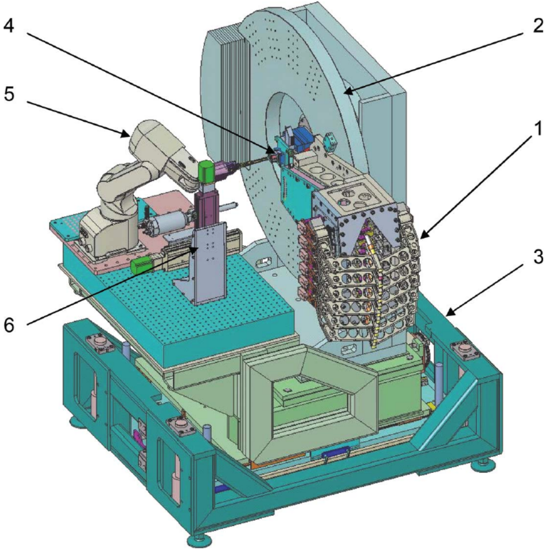

High throughput is obtained using a robot arm to change samples

"A twelve-analyzer detector system for high resolution powder diffraction," P.L. Lee et al. *J. Synch. Rad.* **15**, 427-432

The high resolution analyzer

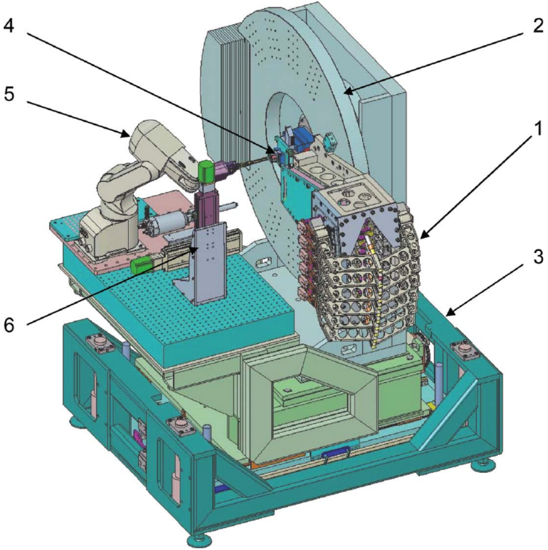

High throughput is obtained using a robot arm to change samples

The sample is mounted on a rotating spindle at the center of the goniometer

"A twelve-analyzer detector system for high resolution powder diffraction," P.L. Lee et al. *J. Synch. Rad.* **15**, 427-432

The high resolution analyzer

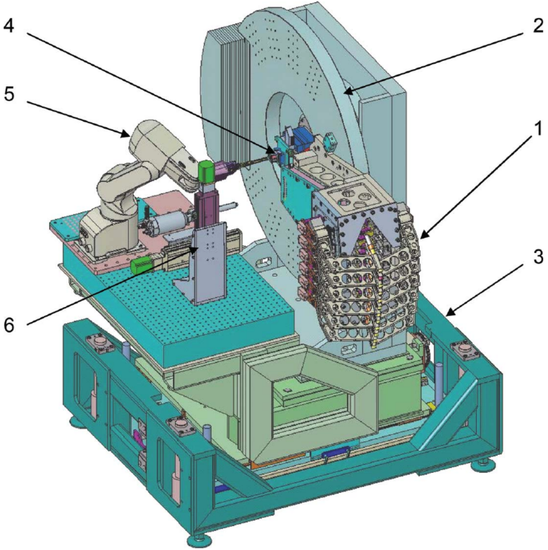

High throughput is obtained using a robot arm to change samples

The sample is mounted on a rotating spindle at the center of the goniometer

High resolution is achieved with a 12 crystal analyzer system which is rotated on the main circle of the goniometer

"A twelve-analyzer detector system for high resolution powder diffraction," P.L. Lee et al. *J. Synch. Rad.* **15**, 427-432

The high resolution analyzer

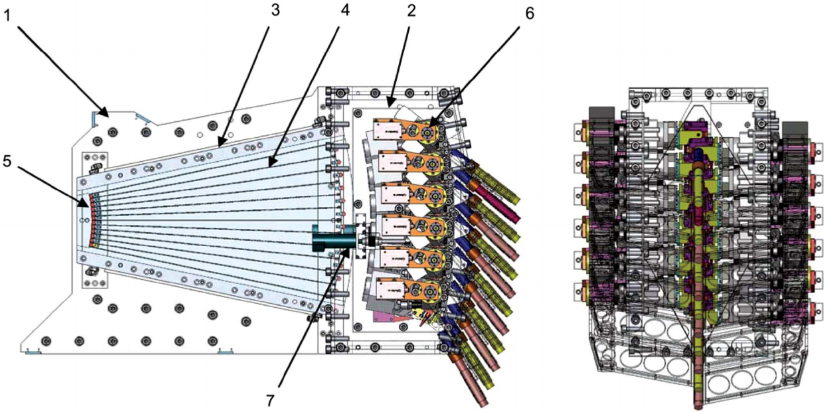

"A twelve-analyzer detector system for high resolution powder diffraction," P.L. Lee et al. *J. Synch. Rad.* **15**, 427-432

The high resolution analyzer

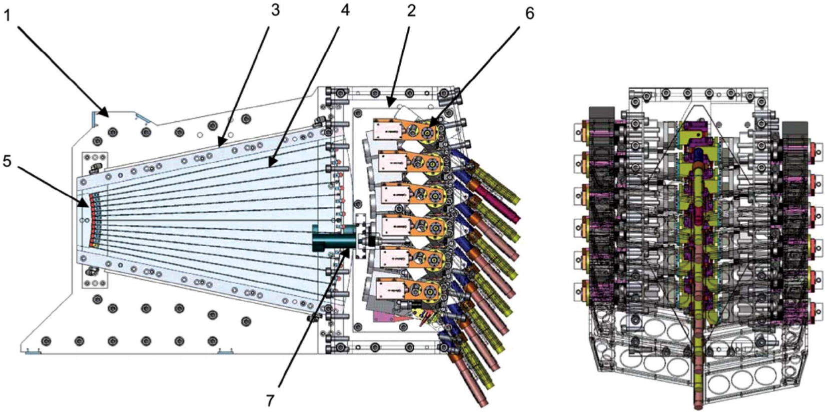

Each of the 12 analyzer crystals is tuned to the desired scattering energy and as the entire assembly is scanned, all twelve banks are collecting data and then are merged

"A twelve-analyzer detector system for high resolution powder diffraction," P.L. Lee et al. *J. Synch. Rad.* **15**, 427-432

The analyzer and robot arm

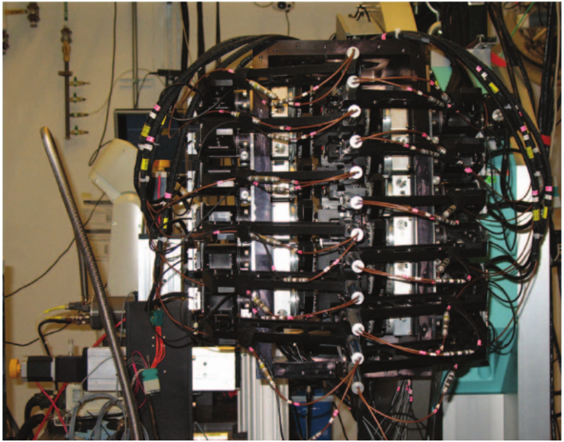

"A twelve-analyzer detector system for high resolution powder diffraction," P.L. Lee et al. *J. Synch. Rad.* **15**, 427-432

The analyzer and robot arm

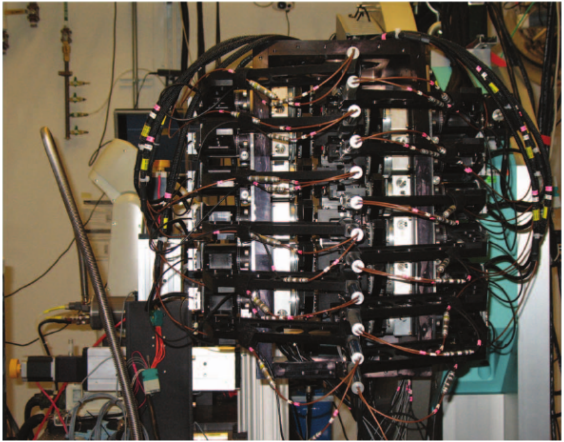

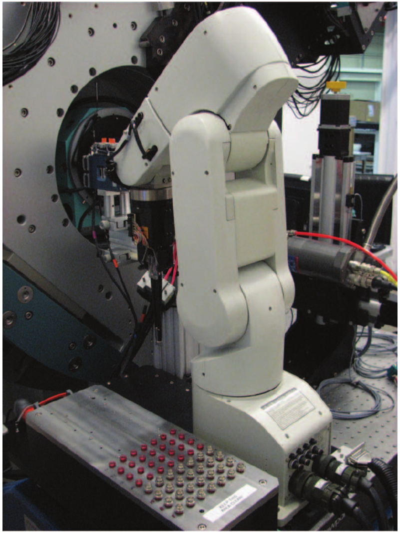

Samples are in Kapton capillaries and magnetic bases for remote mounting

"A twelve-analyzer detector system for high resolution powder diffraction," P.L. Lee et al. *J. Synch. Rad.* **15**, 427-432

Data from high resolution LaB_6 standard

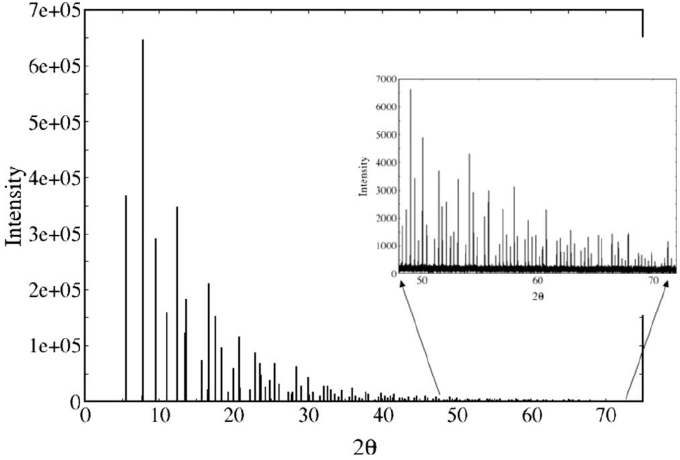

"A dedicated powder diffraction beamline at the Advanced Photon Source: Commissioning and early operational results," J. Wang et al. *Rev. Sci. Instrum.* **79**, 085105 (2008).

Data from high resolution LaB_6 standard

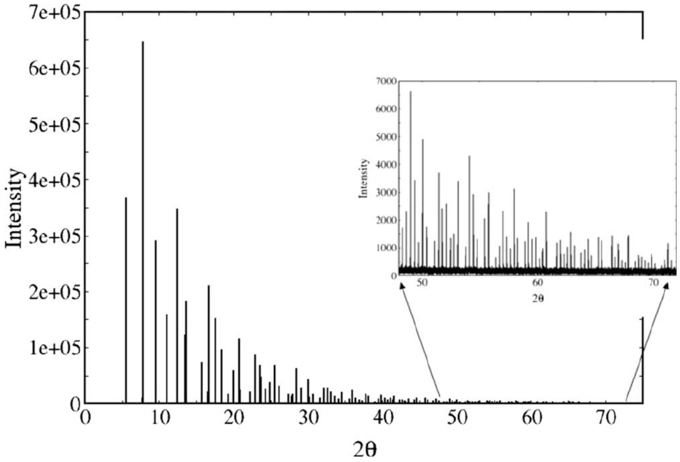

High resolution data with high count rates can be obtained out to very high angles with a wavelength of $\lambda \approx 0.5$Å.

"A dedicated powder diffraction beamline at the Advanced Photon Source: Commissioning and early operational results," J. Wang et al. *Rev. Sci. Instrum.* **79**, 085105 (2008).

Refinement of SiO_2 and Al_2O_3

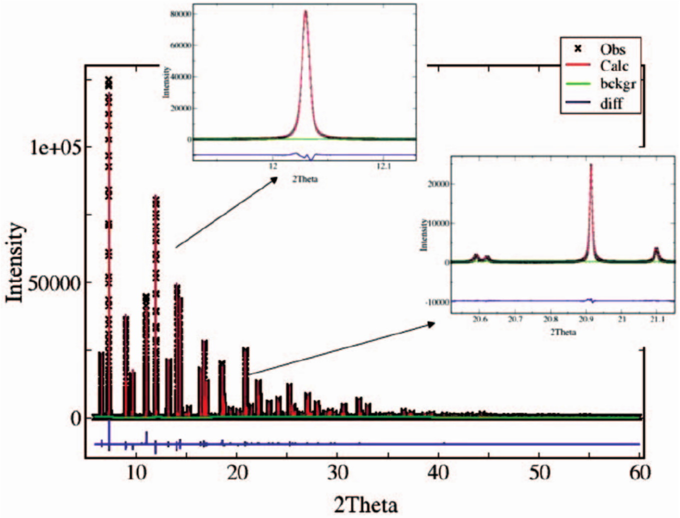

"A dedicated powder diffraction beamline at the Advanced Photon Source: Commissioning and early operational results," J. Wang et al. *Rev. Sci. Instrum.* **79**,